# Bandwidth Estimation of HDD Actuators Using Time Delay Identification

Tetsuo Semba, Fu-Ying Huang, and Matthew T. White

***Abstract*— A method to estimate the maximum achievable bandwidth of HDD actuators without closing the servo loop is presented. The actuator dynamics are characterized by the time delay created by the unstable zeros of the actuator dynamics. The achievable bandwidth is a simple function of the time delay and the sampling frequency. The feedback controller, including a notch filter, can be designed simultaneously. Effects of dynamics variation of the actuator are also considered, and a method to identify the time delay caused by the variation is provided by using the recursive least square method. By applying this method to a single-stage and a dual-stage actuator system of HDDs, it is observed that the variations of the high frequency modes play an important role in the bandwidth improvement, especially of the dual-stage actuator.**

## I. Introduction

Higher-bandwidth servo/mechanical designs are required to increase the track densities of hard disk drives (HDDs). With a mechanical design approach, new types of actuators [1], [2] and some modifications are pursued [3], [4]. With a servo controller design approach, an $H_\infty$ controller design method [5] and a multi-rate sampling technique [6] have been proposed. However, it is not clear how much improvement can be obtained by these techniques before the actuators are made and the servo loops are actually closed. The servo controller design and the bandwidth estimation were possible to achieve in the past by modeling the rigid body mode and the butterfly mode of the actuator, but as the target bandwidth and the sampling frequency increase, accurate bandwidth estimation is not possible without modeling the higher frequency modes. Even a dual-stage actuator will not be an exception to this trend.

Integrated servo/mechanical design is an approach to design the optimum actuator and servo controller at the same time [7], [8]. It has been shown that the FFSPR (Finite frequency strictly positive real) property determines the actuator performance when the performance is evaluated by the tracking error and the magnitude of the control input. A new concept of an actuator based on the FFSPR property has been proposed in [9]. However, for HDD applications, it is desirable to increase the zero-crossover frequency of the open loop transfer function without considering the limit of the control input. This is because the control input for the tracking case is much smaller than for the seeking case, so control input amplitudes for the tracking case are typically ignored.

T. Semba, F-Y. Huang, and M. T. White are with Hitachi Global Storage Technologies, San Jose Research Center, 650 Harry Road, San Jose, CA 95120 USA Tetsuo.Semba@hgst.com, Fu-ying.Huang@hgst.com, and Matthew.White@hgst.com

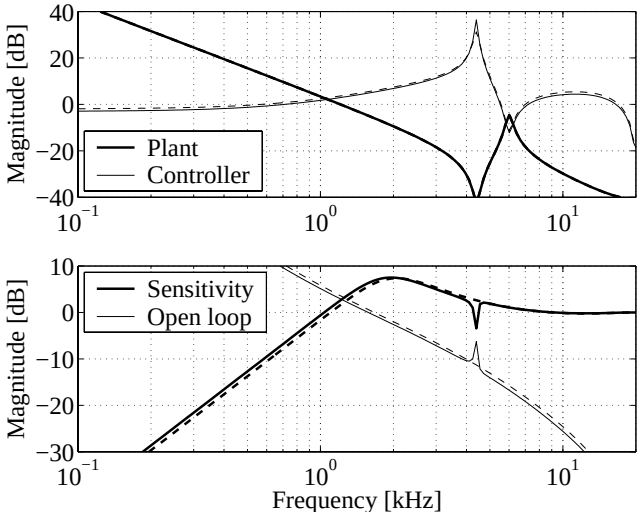


Fig. 1. Transfer functions of $H_\infty$ design results for plants with stable zeros (dotted line) and with unstable zeros (solid line)

This article discusses what characteristics are necessary for the servo/mechanics to achieve higher bandwidth and a technique to design the servo controller and the notch filters to suppress high frequency modes. By using this approach, the bandwidth of a particular actuator design can be estimated before the actuator is actually made, and efficient optimization of the servo and actuator design can be done at the design phase. This approach also helps to estimate how much the bandwidth is degraded when the actuator modes vary. It enables the design of the optimum servo controller and notch filters at the same time with considerations of the tradeoff between the performance and the filter complexity.

## II. Characterization of HDD actuators

$H_\infty$ control theory has been applied for HDD servo controller design to achieve higher bandwidth [4]. Fig. 1 shows an example of transfer functions designed by $H_\infty$ for the plant having a pole at 6 kHz and a zero at 4.4 kHz. The solid line shows the case of an unstable zero and the dashed line shows the case of a stable zero at 4.4 kHz. The plant transfer function for the case with the stable zero is perfectly compensated to eliminate the modes by the pole/zero cancellation. However for the case with the unstable zero, a component remains uncancelled, because the unstable zero cannot be cancelled by an unstable pole. The design results

0-7803-8335-4/04/$17.00 ©2004 AACC

of $H_\infty$ control tend to cancel stable modes and to shape the sensitivity function close to a desired curve as much as possible. Therefore, if a plant has only stable poles and zeros and the robustness against dynamics variation is not important, any servo bandwidth can be obtained by the continuous-time domain approach. By the discrete-time domain approach, the servo bandwidth is only limited by the sampling frequency and the computational delay [10]. If a plant has unstable zeros, the resulting servo bandwidth is limited by the sampling frequency and the unstable zeros as shown in Fig. 1 [11].

According to the Bode Integral Theorem and its extensions, the negative area of the sensitivity function is limited by the positive area [12].

$$\sum_{i=1}^{m} \log |\beta_i| = \frac{1}{\pi} \int_0^{\pi} \log |S(e^{j\phi})| d\phi, \tag{1}$$

where $\beta_i$ are the open-loop unstable poles and $S$ is the sensitivity function of the system. In the case of the HDD servo, since the disturbances to be suppressed are generally located at low frequency, the negative area of the sensitivity function needs to be increased to achieve higher track density. However, if there is a negative area in the high frequency region as shown by the solid line in Fig. 1 around 4.4 kHz, this will be a waste of limited servo capability. It will also increase the positive area that amplifies the sensor noise or decrease the negative area at the low frequency. The desired sensitivity function is the case of stable zeros (dashed line) in Fig. 1. It is inversely proportional to the disturbance at low frequency, such as $s^2$. The sensitivity function at high frequencies slowly decays to zero as the frequency increases. This characteristic is important to have good robustness, because the modes at these frequencies tend to vary.

Assuming the actuator dynamics are denoted by $P(s)$, the numerator of $P(s)$ is divided into the factors of unstable zeros $N_p^+(s)$ and stable zeros $N_p^-(s)$. It is rewritten as

$$P(s) = \frac{N_p^+(s) N_p^-(s)}{D_p(s)}. \tag{2}$$

When the plant is augmented by the poles that are symmetric about the imaginary axis to the unstable zeros, the plant consists of an all-pass filter and a stable factor.

$$\frac{P(s)}{N_p^+(-s)} = \frac{N_p^+(s)}{N_p^+(-s)} \frac{N_p^-(s)}{D_p(s)} \tag{3}$$

The all-pass filter $N_p^+(s)/N_p^+(-s)$ has 0 dB gain over the entire frequency range with some phase change with frequency. Since transfer functions of HDD actuators have unstable zeros in the robustness margin range shown in Fig. 1, the phase change at the low frequency where the bandwidth is determined is approximated by the constant time delay $T_d$. Therefore,

$$\frac{P(s)}{N_p^+(-s)} \approx e^{-sT_d} \frac{N_p^-(s)}{D_p(s)}. \tag{4}$$

This implies that unstable pole/zero cancellation for arbitrary actuator dynamics can be avoided by the introduction of $T_d$, and the sensitivity function is freely manipulated under the constraints of $T_d$. For example, arbitrary $P(s)$ can be converted to a double integrator with some time delay by using a factor $H_c(s)$,

$$P'(s) = P(s) H_c(s) \tag{5}$$

$$\approx \frac{e^{-sT_d}}{s^2}, \tag{6}$$

where

$$H_c(s) = \frac{D_p(s)}{N_p^+(-s) N_p^-(s) s^2} \tag{7}$$

and it has stable poles and zeros except at $s = 0$. Thus, the open loop transfer function of an arbitrary system is approximated by a double integrator, a time delay, and a feedback controller.

The resulting performance is determined by the parameter $T_d$. In this approach $H_c(s)$ becomes a part of the feedback controller. That is, if the controller $C'(s)$ is obtained for the plant with time delay $P'(s)$, the controller for the actual plant $P(s)$ will be $C(s) = H_c(s) C'(s)$. Since the parameter $T_d$ is created by the unstable zeros of the actuator, it is obvious that the optimization of the frequency and the damping of these modes is very important to yield the maximum performance of the actuator.

## III. Controller for a plant with time delay

The performance of the plant in the continuous time domain generalized by (6) is determined only by $T_d$. However, for the discrete-time domain, the performance is determined by both $T_d$ and the sampling frequency $F_s$. By using the $H_\infty$ design method, the feedback controllers $C'(s)$ and the open loop transfer functions are calculated for the plant $P'(s)$ and shown in Fig. 2. An iterative gain adjustment of the weighting functions is performed in the $H_\infty$ design to satisfy the stability margins of 5 dB and 30 °. The maximum achievable zero-crossover frequency of the open loop is a simple function of $T_d$ and $F_s$. For $F_s = 40$ kHz, the zero-crossover frequency is approximated by

$$F_{bw} = \frac{1}{6.0 \times T_d + 170 \times 10^{-6}}, \tag{8}$$

and for $F_s = 80$ kHz

$$F_{bw} = \frac{1}{6.3 \times T_d + 70 \times 10^{-6}}. \tag{9}$$

The difference in the coefficients is due to the fact that the poles can be located higher when the sampling frequency is higher. It is notable that the plant with large time delay will not have higher bandwidth even if the sampling frequency is increased.

By using Fig. 2, the achievable bandwidth of particular actuators can be easily estimated before the servo is closed. The servo controller is designed at the same time by $C(s) = H_c(s) C'(s)$, where $C'(s)$ is a function of $T_d$

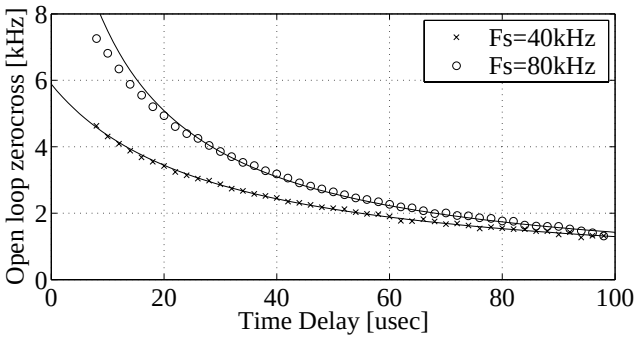


Fig. 2. Maximum achievable zero-crossover frequency of the open loop as a function of time delay and sampling frequency when the design criteria is set to 5 dB and 30 ° margins.

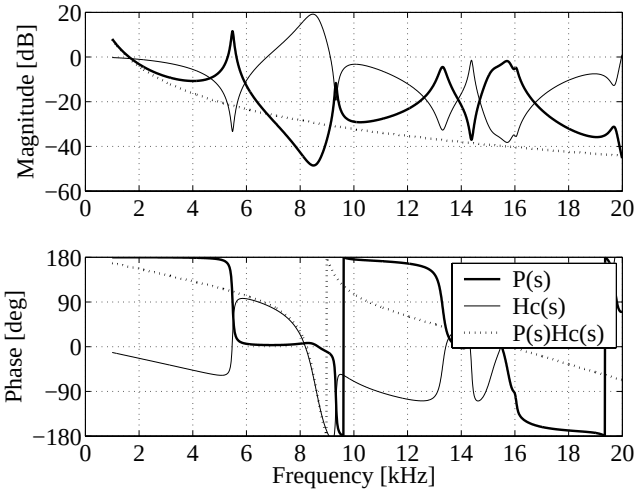


Fig. 3. Transfer functions of VCM actuator obtained by FEM $P(s)$, the shaping filter $H_c(s)$, and the shaped $P'(s) = P(s)H_c(s)$.

and $F_s$. Fig. 3 shows the example of transfer functions for the case of the VCM (Voice Coil Motor) actuator transfer function obtained from a FEM (Finite-Element Method). This actuator has unstable zeros at 8.6 kHz. The phase change at this frequency is observed on the compensated transfer function $P'(s)$ in Fig. 3, because the unstable zero was not fully canceled by the pole.

## IV. Consideration of plant characteristics variation

### A. Shaping filter

Since the actuator dynamics of an actual HDD are not always constant, the optimum $H_c(s)$ designed for a particular actuator is not always robust for another actuator. For example, one HDD has several heads and the transfer functions from the VCM to the various heads are not the same. When the same controller is used for all heads, the controller has to be robust enough for all of the different transfer functions. This must also hold true when the actuator dynamics change with temperature. The time delay approach that has been previously described is also applicable to dynamics that have variations. This relies upon the fact that if the plant transfer function is shaped to be lower than the $1/s^2$ characteristics at the frequencies above the bandwidth $\omega \geq \omega_{bw}$, the robustness will be guaranteed no matter what the phase at these frequencies is. (This is a good assumption for a HDD actuator, but is not necessarily true for any actuator.) That is, if

$$|P_n(\omega)H_c(\omega)| \leq |1/\omega^2|, \omega \geq \omega_{bw} \tag{10}$$

is satisfied for all plant dynamics $P_n(\omega)$, and the controller calculated by the $H_c$ will stabilize all $P_n$.

The design process is as follows. First,

$$P_m(\omega) = \max\{|P_1(\omega)|, \cdots, |P_N(\omega)|\} \tag{11}$$

for each frequency $\omega$ is calculated and $H_c(\omega)$ that satisfies

$$|H_c(\omega)| \leq |\omega^2 P_m(\omega)|^{-1} \tag{12}$$

is obtained by using the frequency domain identification method [13]. If the left hand and the right hand of the formula are close to identical, the time delay of $H_c$ is minimal. Higher order modeling leads to better identification, but the controller including notch filters will be more complex. The tradeoff between the complexity of the feedback controller and the performance is evident at this stage of the design.

### B. Delay time identification in frequency domain

In order to calculate the time delay the model of the maximum envelope of the plant transfer function $P_m(\omega)$ is identified by the Recursive Least Square (RLS) method [13]. In conventional frequency domain identification method, the parameters to be identified are complex numbers, thus the number of parameters is large [14]. However in this application, since the model $H_c(s)$ is minimum phase, the phase information is not necessary. Thus, the algorithm is largely simplified and better accuracy is obtained.

Before the RLS method is applied, an initial model of the transfer function has to be obtained, because in any method of the recursive computation, initial values are important to have good convergence as well as accuracy. The initial model is formulated by the following

$$P_{init}(s) = \sum_{l=0}^{N-1} \frac{k_l}{s^2 - 2\zeta_l\omega_l s + \omega_l^2}. \tag{13}$$

Since the peaks of $P_{init}(s)$ roughly correspond to the gain and the damping of each term, the initial values of $k_l$, $\zeta_l$, and $\omega_l$ are obtained by

1) Calculate maximum magnitude $P_m(\omega_j)$ around the neighborhood of $\omega_j - \delta\omega \leq \omega < \omega_j + \delta\omega$ to get the maximum envelope and to eliminate the small change.
2) Look for peaks by checking $P_m(\omega_j) \geq P_m(\omega_j - \delta\omega)$ and $P_m(\omega_j) > P_m(\omega_j + \delta\omega)$ for all frequencies $\omega_j$.
3) When there is a peak at $\omega_j$, then $\omega_l \cong \omega_j$ and the damping ratio $\zeta_l$ can be approximately calculated using the magnitude change in the neighborhood.

4) The residue gain $k_l$ is calculated by $k_l \cong 2\omega_l\zeta_l P_m(\omega_l)$.

Thus the intial model $P_{init}(s)$ is obtained. The order of the model can be changed by modifying $\delta\omega$. When it is smaller, a higher order model can be obtained, but the computation time becomes longer.

For the RLS method, a multiplicative plant model is used because of the simplicity of the Jacobian matrix. The initial model is also converted to the following form to define the initial parameters

$$P(s) = \frac{k\prod_{n=0}^{N-2}(s-a_n+jb_n)(s-a_n-jb_n)}{\prod_{n=0}^{N-1}(s-c_n+jd_n)(s-c_n-jd_n)}. \quad (14)$$

Let $f(s) = \log|P(s)|$ and unknown parameters

$$\boldsymbol{\theta} = (\log k, a_0, ...a_{N-2}, b_0, ...b_{N-2}, c_0, ...c_{N-1}, d_0, ...d_{N-1})^T \quad (15)$$

then

$$\begin{aligned} f(\omega) &= \log k \\ &+ \frac{1}{2}\sum_{n=0}^{N-2}\log\left((a_n^2+b_n^2)^2+2(a_n^2-b_n^2)\omega^2+\omega^4\right) \\ &- \frac{1}{2}\sum_{n=0}^{N-1}\log\left((c_n^2+d_n^2)^2+2(c_n^2-d_n^2)\omega^2+\omega^4\right). \end{aligned}$$

The Jacobian $\boldsymbol{J}$ is

$$J_{ij} = \frac{\partial f_j(\boldsymbol{\theta})}{\partial\theta_i}, \quad (16)$$

and

$$\begin{aligned} \frac{\partial f(\omega)}{\partial \log k} &= 1 \\ \frac{\partial f(\omega)}{\partial a_n} &= \frac{2a(a_n^2+b_n^2+\omega^2)}{(a_n^2+b_n^2)^2+2(a_n^2-b_n^2)\omega^2+\omega^4} \\ \frac{\partial f(\omega)}{\partial b_n} &= \frac{2b(a_n^2+b_n^2-\omega^2)}{(a_n^2+b_n^2)^2+2(a_n^2-b_n^2)\omega^2+\omega^4} \\ \frac{\partial f(\omega)}{\partial c_n} &= \frac{-2c(c_n^2+d_n^2+\omega^2)}{(c_n^2+d_n^2)^2+2(c_n^2-d_n^2)\omega^2+\omega^4} \\ \frac{\partial f(\omega)}{\partial d_n} &= \frac{-2d(c_n^2+d_n^2-\omega^2)}{(c_n^2+d_n^2)^2+2(c_n^2-d_n^2)\omega^2+\omega^4}. \end{aligned}$$

The parameter offset for the update is

$$\Delta\boldsymbol{\theta} = (\boldsymbol{J}^T\boldsymbol{J}+\lambda\boldsymbol{I})^{-1}\boldsymbol{J}^T(\boldsymbol{y}-\boldsymbol{f}(\boldsymbol{\theta})), \quad (17)$$

where $\boldsymbol{y} = \log|P_m(\boldsymbol{\omega})|$ is the set the measured maximum envelope of the transfer function. (See the appendix for details.) The parameter update (17) is repeated by $\boldsymbol{\theta} + \Delta\boldsymbol{\theta} \rightarrow \boldsymbol{\theta}$ until the result converges. During the iteration $\lambda$ is adjusted based on the error. When the initial model is far from the actual, $\lambda$ is set to be larger and convergence is faster. When the error becomes smaller, $\lambda$ is set to be smaller to achieve better accuracy.

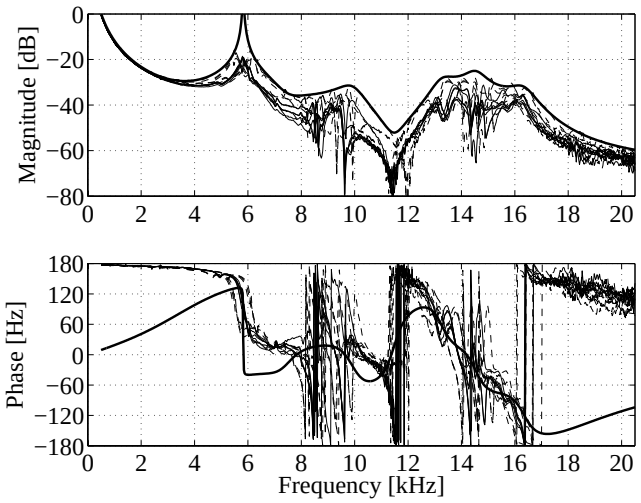


Fig. 4. Plant transfer functions (dotted lines) and identified transfer function of maximum envelope (solid line).

The resulting shaping filter is

$$H_c(s) = \frac{1}{s^2P(\boldsymbol{\theta})}. \quad (18)$$

When the resulting $H_c(s)$ is non-minimum phase, the pole and zeros have to be converted to have the minimum phase property. The approximated time delay $T_d$ can be obtained by

$$\begin{aligned} T_d &\cong -\frac{d\angle P(\omega)}{d\omega}|_{\omega\rightarrow 0} \\ &\cong \sum_{j=0}^{N-1}\frac{2c_j}{c_j^2+d_j^2} - \sum_{j=0}^{N-2}\frac{2a_j}{a_j^2+b_j^2}. \end{aligned}$$

According to this equation, when the mode frequency is lower, the bandwidth tends to become lower, because the time delay becomes larger. This explains the empirical rule that the butterfly mode frequency of an actuator needs to be increased for higher servo bandwidth.

## V. Design results

Fig. 4 shows the measured transfer functions for the 12 heads of the VCM with ±3 dB and ±300 Hz mode variation $P_n(s), (n = 1, \cdots, 12)$ and the identified transfer function $P(\boldsymbol{\theta})$ from their maximum envelope. Fig. 5 shows the plant transfer functions with the shaping filter $P_n(s)H_c(s)$ (dotted lines) and the $1/s^2$ characteristics (solid line). The envelope of the maximum transfer function matches the $1/s^2$ curve and some phase delay is introduced by the shaping filter.

The shaping filter $H_c$ and the time delay $T_d$ are calculated for a VCM actuator with 12 heads and a moving-suspension-type dual-stage actuator. The dynamics variation is assumed for 12 heads with ±3 dB gain and ±300 Hz frequency variations for all modes. Fig. 6 shows the open loop transfer functions $P_n(s)C(s)$, the sensitivity functions $S_n(s) = (1+P_n(s)C(s))^{-1}$, and the controller including the notch filter $C(s)H_c(s)$ for the VCM actuator. Fig.

TABLE I

TIME DELAY AND MAXIMUM OPEN LOOP BANDWIDTH OF ACTUATORS WITH AND WITHOUT DYNAMICS VARIATION.

| *Actuator* | Dynamics Variation | Delay $T_d$ [$\mu$s] | Bandwidth [Hz] ($F_s$ =40kHz) | Bandwidth [Hz] ($F_s$ =80kHz) |
|---|---|---|---|---|
| *Single-stage VCM of one head (calculated by FEM)* | 0 dB, 0 Hz | 32 | 2760 (2550) | 3680 (3300) |
| *Single-stage VCM of 12 heads (measured by LDV)* | 0 dB, 0 Hz | 56 | 1980 (1870) | 2370 (2200) |
| | $\pm$3 dB, $\pm$300 Hz | 61 | 1870 (1770) | 2200 (2060) |
| *Dual-stage of one head (calculated by FEM)* | 0 dB, 0 Hz | 4.5 | 5080 (4410) | 10000 (7700) |
| | $\pm$3 dB, $\pm$300 Hz | 32 | 2760 (2550) | 3680 (3300) |

Numbers in brackets are the bandwidth assuming the computational delay of 5 $\mu$s.

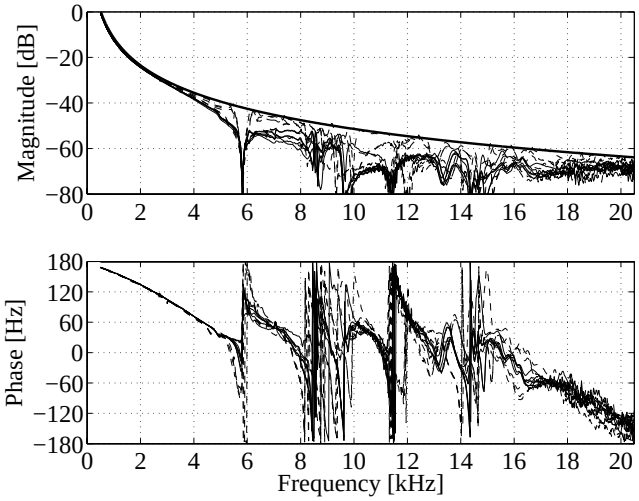


Fig. 5. Plant transfer functions with shaping filter (dotted lines) and the $1/s^2$ characteristics (solid line).

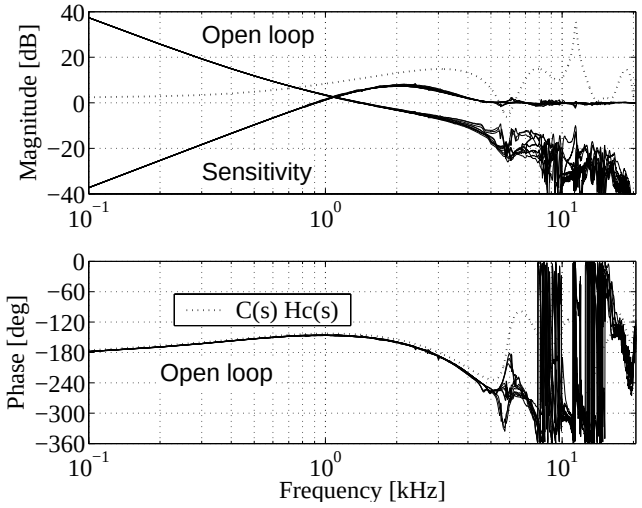


Fig. 6. Open loop transfer functions and sensitivity functions obtained for the 12 heads of the VCM with $\pm$3 dB and $\pm$300 Hz mode variation.

7 shows the case for the moving-suspension-type dual-stage actuator system. These transfer functions are stabilized by the controller obtained by the method in the previous section, and the achievable bandwidth is estimated by Fig. 2. The only necessary parameter is the time delay $T_d$ based on $H_c(s)$.

Table I summarizes the time delay and the achievable bandwidth of various situations for the VCM actuator and a moving-suspension-type dual-stage actuator. In the case of the VCM, the variation does not affect the bandwidth very much, because the time delay without the variation is already large. However, for the dual-stage actuator, the bandwidth varies by 2-3 times compared to the case without the dynamics variation. This is because the time delay of the dual-stage actuator is more dominated by the dynamics variation than the unstable zeros. This implies that the performance of a moving-suspension-type actuator heavily depends on the high frequency mode characteristics. In order to achieve much higher bandwidth of HDD servo, a clean transfer function without dynamics variation at high frequency is necessary even for a dual-stage actuator.

## VI. CONCLUSIONS

A method to estimate the maximum achievable bandwidth of a HDD actuator is presented. A time delay is introduced when the plant transfer function is shaped to match double integrator characteristics using a stable, minimum-phase compensator. This delay is created by the unstable zeros of the actuator dynamics. The performance of the actuator without dynamics variations can be determined by this factor. A mechanical design for a high-bandwidth actuator can be achieved when the time delay is minimal. The feedback controller, including the notch filter, is designed by this method. The performance with dynamics variations can be also evaluated, which demonstrates the tradeoff between the performance and the controller complexity. This method was applied to a servo design for a conventional actuator as well as a moving-suspension-type dual-stage actuator. This design showed that the variations of the high frequency modes played an important role for the improvement of the bandwidth of the dual-stage system.

## REFERENCES

[1] T. Semba, T. Hirano, J. Hong, L. S. Fan,"Dual-Stage Servo Controller for HDD Using MEMS Microactuator," IEEE Trans. Mag., 35-5, pp. 2271-2273 (1999)

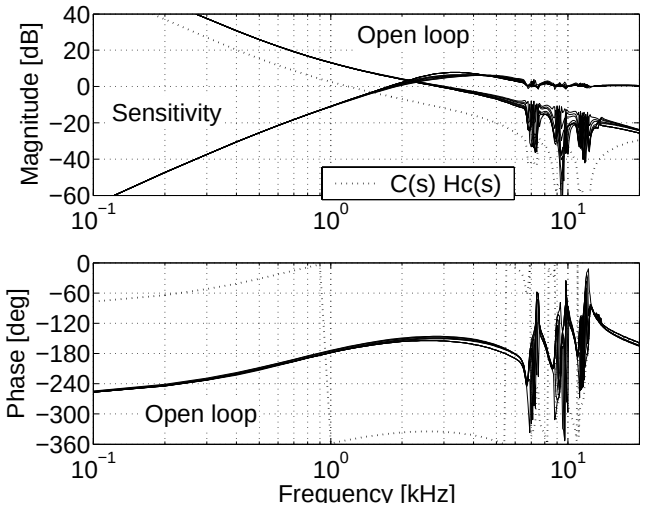


Fig. 7. Open loop transfer functions and sensitivity functions obtained for the dual-stage actuator with $\pm 3$ dB and $\pm 300$ Hz mode variation.


[2] K. Mori, T. Munemoto, H. Ohtsuki, Y. Yamaguchi, K. Akagi, "A Dual-Stage Magnetic Disk Drive Actuator Using a Piezoelectric Device for a High Track Density," IEEE Trans. Mag., Vol. 27, pp. 5298-5300, Nov. 1991.

[3] F. Huang, "FEM-Assisted Analytical Model for Rotary Actuator Dynamics," ASME Symp. ISPS, Santa Clara, Jun. 1999.

[4] S. Nakagawa, M. Kobayashi, T. Yamaguchi, "A Higher Bandwidth Servo Design with Strain Feedback Control for Magnetic Disk Drives," Proc. of ACC, pp. 2547-2552, Jun. 2003.

[5] M. Hirata, K. Z. Liu, T. Mita, and T. Yamaguchi "Head Positioning Control of a Hard Disk Drive Using H-infinity Theory," Proc. of CDC, pp. 2460-2461, Dec. 1992.

[6] W-W. Chiang, "Multirate State-Space Digital Controller for Sector Servo System," Proc. of CDC, pp. 1902-1907, Dec. 1990.

[7] T. Iwasaki, "Integrated System Design by Separation," Proc. IEEE Int. Conf. on Contr. Appl., pp. 97-102, Aug. 1999.

[8] S. Hara, M. Nishio, and T. Maruyama, "Integrated Design for High Robust Performance with Quick Time-Response," Proc. IEEE Int. Conf. on Contr. Appl., pp. 176-181, Aug. 1999.

[9] T. Iwasaki, S. Hara, and H. Yamauchi, "Structure/Control Design Integration with Finite Frequency Positive Real Property," Proc. of ACC, pp. 549-553, Jun. 2000.

[10] M. T. White, and W-M. Lu, "Hard Disk Drive Bandwidth Limitations Due to Sampling Frequency and Computational Delay," Proc. of IEEE/ASME Int. Conf. on Advanced Intelligent Mechatronics, pp. 120-125, Sep. 1999.

[11] J. S. Freundenburg, and D. P. Looze, "Right Half Plane Poles and Zeros and Design Tradeoffs in Feedback Systems," IEEE Trans. on Automatic Control, Vol. AC-30, No. 6, pp. 555-565, Jun. 1985.

[12] C. Mohtadi, "Bode's Integral Theorem for Discrete-Time Systems," IEE Proc., Vol. 137, Pt. D, No. 2, pp. 57-66, 1990.

[13] J. Schoukens and R. Pintelon, *Identification of Linear Systems*, Pergamon Press, 1991.

[14] M. Kawafuku, K. Otsu, H. Hirai, M. Kobayashi, "High Performance Controller Design of HDD Based on Precise System Modeling Using Differential Iteration Method," Proc. of ACC, pp. 4341-4346, Jun. 2003.


## APPENDIX

### *Parameter identification by RLS Method [13]*

The cost function to be minimized is the squared error between the magnitude of the measured data $y(\omega_j)$ and the model output $f_j$

$$K(\boldsymbol{\theta}) = \sum_{j=1}^{m} \left(y(\omega_j) - f_j(\boldsymbol{\theta})\right)^2, \tag{A.1}$$

where $f_j(\boldsymbol{\theta})$ is the data calculated by the model parameters $\boldsymbol{\theta}$ at each frequency $\omega_j$. Since $f_j(\boldsymbol{\theta})$ is a nonlinear function of $\boldsymbol{\theta}$, the cost function is minimized by the recursive least square (RLS) method. The 2nd-order partial derivative of the cost function is

$$\frac{\partial^2 K}{\partial \boldsymbol{\theta}^2} = 2\sum_{j=1}^{m}\left(\left(\frac{\partial f_j}{\partial \boldsymbol{\theta}}\right)^T\left(\frac{\partial f_j}{\partial \boldsymbol{\theta}}\right) - \left(y(\omega_j) - f_j\right)\frac{\partial^2 f_j}{\partial \boldsymbol{\theta}^2}\right). \tag{A.2}$$

Since the 2nd term of the right side is smaller than the 1st term,

$$\frac{\partial^2 K}{\partial \boldsymbol{\theta}^2} \cong 2\sum_{j=1}^{m}\left(\frac{\partial f_j}{\partial \boldsymbol{\theta}}\right)^T\left(\frac{\partial f_j}{\partial \boldsymbol{\theta}}\right) = 2\boldsymbol{J}^T\boldsymbol{J}, \tag{A.3}$$

where

$$\boldsymbol{J} = \frac{\partial \boldsymbol{f}}{\partial \boldsymbol{\theta}}. \tag{A.4}$$

When the parameter is $\boldsymbol{\theta}$ at some point of iteration, a new cost function when the parameter $\boldsymbol{\theta}$ is shifted by $\Delta\boldsymbol{\theta}$ can be expressed by the Taylor's expansion.

$$K(\boldsymbol{\theta} + \Delta\boldsymbol{\theta}) = K(\boldsymbol{\theta}) + \frac{\partial K}{\partial \boldsymbol{\theta}}\Delta\boldsymbol{\theta} + \frac{1}{2}\Delta\boldsymbol{\theta}^T\frac{\partial^2 K}{\partial \boldsymbol{\theta}^2}\Delta\boldsymbol{\theta} + \ldots \tag{A.5}$$

A necessary condition for having an extreme for $K$ in $\boldsymbol{\theta} + \Delta\boldsymbol{\theta}$ is that the derivative with respect to $\Delta\boldsymbol{\theta}$ in $\boldsymbol{\theta} + \Delta\boldsymbol{\theta}$ should be equal to zero, so

$$\left(\frac{\partial K(\boldsymbol{\theta} + \Delta\boldsymbol{\theta})}{\partial \Delta\boldsymbol{\theta}}\right)^T_{|\Delta\boldsymbol{\theta}} = \frac{\partial K(\boldsymbol{\theta})}{\partial \boldsymbol{\theta}}^T_{|\boldsymbol{\theta}} + \frac{\partial^2 K(\boldsymbol{\theta})}{\partial \boldsymbol{\theta}^2}_{|\boldsymbol{\theta}}\Delta\boldsymbol{\theta}. \tag{A.6}$$

The solution of this linear equations gives the value of $\Delta\boldsymbol{\theta}$

$$\Delta\boldsymbol{\theta} = -\left(\frac{\partial^2 K}{\partial \boldsymbol{\theta}^2}\right)^{-1}\left(\frac{\partial K}{\partial \boldsymbol{\theta}}\right)^T. \tag{A.7}$$

The 1st-order derivative in this equation is obtained from (A.1)

$$\left(\frac{\partial K}{\partial \boldsymbol{\theta}}\right)^T = -2\boldsymbol{J}^T\left(\boldsymbol{y} - \boldsymbol{f}(\boldsymbol{\theta})\right). \tag{A.8}$$

The results of the Gauss-Newton method is from (A.3), (A.7), and (A.8)

$$\Delta\boldsymbol{\theta} = (\boldsymbol{J}^T\boldsymbol{J})^{-1}\boldsymbol{J}^T\left(\boldsymbol{y} - \boldsymbol{f}(\boldsymbol{\theta})\right). \tag{A.9}$$

The parameter is updated by $\boldsymbol{\theta} + \Delta\boldsymbol{\theta} \rightarrow \boldsymbol{\theta}$ and (A.9) is repeated until it converges. The method of Levenberg-Marquardt is used to improve the convergence of the recursive algorithm. The modified update equation is

$$\Delta\boldsymbol{\theta} = (\boldsymbol{J}^T\boldsymbol{J} + \lambda\boldsymbol{I})^{-1}\boldsymbol{J}^T\left(\boldsymbol{y} - \boldsymbol{f}(\boldsymbol{\theta})\right). \tag{A.10}$$

By changing $\lambda$ during iteration, faster and better convergence is obtained.